Science
AAAS

Proteome Half-Life Dynamics in Living Human Cells

Eran Eden, *et al.*

Science **331**, 764 (2011);
DOI: 10.1126/science.1199784

1 to 3 with lanes 4 to 6 and lanes 7 to 9 with lanes 10 to 12, and Fig. 4C). These data establish a role for HSPC117 as an RNA ligase with broad substrate specificity and with a function in tRNA processing in living cells.

Both RNA>p ligase and T4 Rnl1–like ligation mechanisms have been detected in human cells (*12*, *27*) but RNA>p ligase seems to play a dominant role in human tRNA splicing (*12*, *28*). We have identified HSPC117 as an essential component of the prevalent human tRNA splicing pathway. Recently, HSPC117 or the RNA>p ligase pathway have also been implicated in RNA processing during viral replication (*29*, *30*). The high degree of conservation of HSPC117/RtcB proteins is suggestive of shared roles for this protein family in organisms as distantly related as humans and *E. coli*.

References and Notes

1. E. M. Phizicky, A. K. Hopper, *Genes Dev.* **24**, 1832 (2010).
2. S. V. Paushkin, M. Patel, B. S. Furia, S. W. Peltz, C. R. Trotta, *Cell* **117**, 311 (2004).
3. C. R. Trotta *et al.*, *Cell* **89**, 849 (1997).
4. J. Abelson, C. R. Trotta, H. Li, *J. Biol. Chem.* **273**, 12685 (1998).
5. M. Englert, H. Beier, *Nucleic Acids Res.* **33**, 388 (2005).
6. M. Konarska, W. Filipowicz, H. Domdey, H. J. Gross, *Nature* **293**, 112 (1981).
7. E. M. Phizicky, R. C. Schwartz, J. Abelson, *J. Biol. Chem.* **261**, 2978 (1986).
8. L. K. Wang, C. K. Ho, Y. Pei, S. Shuman, *J. Biol. Chem.* **278**, 29454 (2003).
9. B. L. Apostol, S. K. Westaway, J. Abelson, C. L. Greer, *J. Biol. Chem.* **266**, 7445 (1991).
10. R. Sawaya, B. Schwer, S. Shuman, *J. Biol. Chem.* **278**, 43928 (2003).
11. W. Filipowicz, M. Konarska, H. J. Gross, A. J. Shatkin, *Nucleic Acids Res.* **11**, 1405 (1983).
12. W. Filipowicz, A. J. Shatkin, *Cell* **32**, 547 (1983).
13. F. A. Laski, A. Z. Fire, U. L. RajBhandary, P. A. Sharp, *J. Biol. Chem.* **258**, 11974 (1983).
14. L. Zofallova, Y. Guo, R. Gupta, *RNA* **6**, 1019 (2000).
15. J. Martinez, A. Patkaniowska, H. Urlaub, R. Lührmann, T. Tuschl, *Cell* **110**, 563 (2002).
16. See supporting material on *Science* Online.
17. O. Vicente, W. Filipowicz, *Eur. J. Biochem.* **176**, 431 (1988).
18. EBI InterPro database entry www.ebi.ac.uk/interpro/IEntry?ac=IPR001233.
19. P. Genschik, K. Drabikowski, W. Filipowicz, *J. Biol. Chem.* **273**, 25516 (1998).
20. M. Y. Galperin, E. V. Koonin, *Nucleic Acids Res.* **32**, 5452 (2004).
21. K. Goyal, S. C. Mande, *Proteins* **70**, 1206 (2008).
22. C. Okada, Y. Maegawa, M. Yao, I. Tanaka, *Proteins* **63**, 1119 (2006).
23. S. Weitzer, J. Martinez, *Nature* **447**, 222 (2007).
24. V. Drewett *et al.*, *Nucleic Acids Res.* **29**, 479 (2001).
25. K. K. Perkins, H. Furneaux, J. Hurwitz, *Proc. Natl. Acad. Sci. U.S.A.* **82**, 684 (1985).
26. M. Englert, K. Sheppard, A. Aslanian, J. R. Yates III, D. Söll, *Proc. Natl. Acad. Sci. U.S.A.* 10.1073/pnas.1018307108 (2011).
27. M. Zillmann, M. A. Gorovsky, E. M. Phizicky, *Mol. Cell. Biol.* **11**, 5410 (1991).
28. H. P. Harding *et al.*, *RNA* **14**, 225 (2008).
29. D. Cao, D. Haussecker, Y. Huang, M. A. Kay, *RNA* **15**, 1971 (2009).
30. C. E. Reid, D. W. Lazinski, *Proc. Natl. Acad. Sci. U.S.A.* **97**, 424 (2000).

31. We thank H. Beier, T. Biederer, T. Clausen, A. Meinhart, A. F. Nielsen, R. Schroeder, K. Sheppard, T. Tuschl, and S. Westermann for reagents and helpful discussions; and G. Heyne, O. Kuzyk, G. Schmauss, and G. Stengl for technical assistance; and H. Urlaub for MS analysis of HSPC117 complexes. M.E. was a Feodor-Lynen Postdoctoral Fellow of the Alexander von Humboldt Stiftung (Bonn, Germany). Supported by grants from the European Commission (EURASNET-518238) (R.L.), the Fonds zur Förderung der wissenschaftlichen Forschung (W1207 RNA Biologie) (J.P.), and the National Institute of General Medical Sciences (D.S.). J.M. would like to especially acknowledge the generous financial contribution and support by S.D. Prinz Max von und zu Liechtenstein.

Supporting Online Material

www.sciencemag.org/cgi/content/full/331/6018/760/DC1
Materials and Methods
Figs. S1 to S10
Tables S1 to S3
References

15 September 2010; accepted 7 January 2011
10.1126/science.1197847

Proteome Half-Life Dynamics in Living Human Cells

Eran Eden,*† Naama Geva-Zatorsky,* Irina Issaeva, Ariel Cohen, Erez Dekel, Tamar Danon, Lydia Cohen, Avi Mayo, Uri Alon†

Cells remove proteins by two processes: degradation and dilution due to cell growth. The balance between these basic processes is poorly understood. We addressed this by developing an accurate and noninvasive method for measuring protein half-lives, called "bleach-chase," that is applicable to fluorescently tagged proteins. Assaying 100 proteins in living human cancer cells showed half-lives that ranged between 45 minutes and 22.5 hours. A variety of stresses that stop cell division showed the same general effect: Long-lived proteins became longer-lived, whereas short-lived proteins remained largely unaffected. This effect is due to the relative strengths of degradation and dilution and suggests a mechanism for differential killing of rapidly growing cells by growth-arresting drugs. This approach opens a way to understand proteome half-life dynamics in living cells.

Protein removal plays a role in numerous cellular processes, including cell cycle regulation, differentiation, apoptosis, and signal transduction (*1*, *2*), and in disease (*3*, *4*). Understanding the principles that govern protein removal is needed to understand how cells regulate their proteome.

Cells remove proteins by two main processes: intracellular degradation (*2*) (e.g., via the proteasome) and dilution, which is due to cell growth, effectively reducing the protein amount by 50% with every division (*5*, *6*). Degradation can selectively regulate individual proteins, whereas changes in dilution rate globally affect the proteome. The balance between these two processes varies across organisms and cell types. In rapidly dividing cells, such as bacteria, dilution is often more dominant than degradation, and thus, growth-rate largely determines the protein removal rate (*6*, *7*). In contrast, nondividing and slowly dividing cells, such as differentiated mammalian cells, seem to rely mostly on degradation, because dilution is negligible. In mammalian cells that undergo moderate cell growth, including cancer cells, a systems-level understanding of the balance between these two fundamental processes is lacking.

Studying protein removal requires a method that should ideally: (i) facilitate measurements of many proteins, (ii) cause minimal interference to the cell, (iii) have high temporal resolution and accuracy, and (iv) work in living cells. A traditional method, "pulse-chase," radioactively labels the protein of interest over a brief period (the pulse), and then the decay in radioactivity is measured over time (the chase) and is used to infer protein half-life (*7*). This assay is accurate and minimally perturbative but requires a specific antibody for each protein and is difficult to scale to multiple proteins. One way to increase throughput is to integrate pulse-chase with mass spectrometry (*5*). However, this approach does not enable real-time monitoring of living cells. Protein synthesis inhibitors have also been used to measure removal rates but lead to severe cell perturbation. Another approach uses dual-fluorescent reporters to estimate relative protein turnover (*8*) but does not supply quantitative half-lives.

We present an assay called "bleach-chase" for measuring protein half-lives that does not require translation inhibitors, antibodies, or radioactive labeling. It can be applied to multiple proteins and time points in living cells and is generally applicable to fluorescently tagged proteins (Fig. 1A). We first provide a description of the idea behind bleach-chase and then turn to experimental tests of the method.

We use the term "degradation" to refer to intracellular processes that lead to proteolysis, such as lysosome- and proteasome-mediated degradation. Protein removal rate, α, is the sum of the degradation, α_{deg}, and the dilution rate, α_{dil} (*6*, *9*)

$$\alpha = \alpha_{deg} + \alpha_{dil} \quad (1)$$

In the bleach-chase method, the fluorophore of the tagged protein is bleached using a brief pulse

Department of Molecular Cell Biology, Weizmann Institute of Science, Rehovot 76100, Israel.

*These authors contributed equally to this work.
†To whom correspondence should be addressed. E-mail: eraneden@gmail.com (E.E.); urialon@weizmann.ac.il (U.A.)

of light, irreversibly rendering it nonfluorescent. It is sufficient to bleach only a small fraction of the tagged proteins to generate two subpopulations of the tagged protein: fluorescent and nonfluorescent. After bleaching, the nonfluorescent proteins are no longer produced and decay at a rate that depends solely on protein removal. Because nonfluorescent proteins are invisible to fluorescence microscopy, we measured them by subtracting the observed fluorescence levels of bleached and unbleached cells (Fig. 1B, Fig. 2A, and movie S1). The protein removal rate α is the slope of decay of the difference between the bleached and unbleached protein fluorescence on a semilogarithmic plot [for details and mathematical analysis, see (*10*)]. The protein half-life, defined as the time for removal of half of the protein, is $T_{1/2} = \ln(2)/\alpha$.

We applied bleach-chase to clones from a library of annotated reporter cell clones, the LARC library of human cancer cells (based on the H1299 human non–small cell lung cancer cell line). The clones express different proteins tagged by yellow fluorescent protein (YFP) as an internal exon at their endogenous loci (*11*, *12*). We followed protein levels using fluorescence time-lapse microscopy and image analysis (Fig. 1A) (*10*, *11*).

YFP fluorophores were bleached by brief (30- to 480-s) pulses of light, resulting in a 10 to 60% decrease in tag fluorescence. Bleaching did not alter cell motility (10.1 ± 1.6 versus 10.3 ± 1.5 μm/hour), cell cycle (22.5 ± 2.6 versus 23.2 ± 2.5 hours), viability, or morphology, in agreement with previous observations that green fluorescent protein (GFP)–fused proteins are relatively nonphototoxic under fluorescence microscopy and retain protein activity under mild bleaching (*13*, *14*). Fluorescence profiles after bleaching converged to nonbleached profiles with exponential dynamics, which revealed the removal rate (Fig. 2B). The day-to-day error in removal rate was about 0.4 [coefficient of variation (CV)]. By averaging more than three or four experiments, we obtained an average error of about 0.25 (CV).

Bleach-chase compared well with radioactive pulse-chase experiments, the gold standard, and showed similar half-lives for tagged proteins (11% median difference, seven proteins) and similar half-lives when comparing tagged proteins to their untagged counterparts (16% median difference, six proteins) (tables S1 to S3 and fig. S2). As a final test of the method, we applied bleaching at different intensities. The measured removal rates remained similar (CV < 0.2), regardless of bleaching intensity (fig. S3). Thus, bleach-chase seems to measure protein removal rates accurately in living cells.

We next asked which process, degradation or dilution, dominates protein removal. We began with growth conditions in which the cells vigorously divided and used bleach-chase to assay 100 proteins spanning different cellular localizations and functions for 24 hours (every 20 min) with three to four day-to-day repeats. We observed a broad protein half-life distribution ranging between 45 min to 22.5 hours, with mean 9.0 ± 4.6 hours (Fig. 2D and table S4). Degradation rates were obtained by subtracting the dilution rate [α_{dil} = 0.03 ± 0.004 1/hour, (*10*)] from the removal rates. Degradation was dominant for 45% of the proteins, dilution was dominant for 12%, and the two were comparable for 43% (Fig. 2E). Thus, how much protein removal depends on degradation or dilution varies widely between proteins. We tested whether this correlates with function and localization (Fig. 2F). Proteins localized to the cytoplasm had higher degradation rates than might be expected by chance (mHG $P < 10^{-4}$) (*10*), as did members of the anaphase-promoting complex (mHG $P < 10^{-2}$) and cell cycle–regulating proteins (mHG $P < 10^{-3}$). In contrast, proteins of the translation-initiation complex tended to be degraded more slowly (mHG $P < 10^{-2}$). Thus, proteins with similar function or localization seemed to rely similarly on either dilution or degradation for their removal.

We next asked how half-lives change under stresses and whether general trends govern these changes. As a case study, we used the anticancer drug camptothecin (CPT) (*11*, *15*), a topoisomerase-1 poison, and measured the half-life of 32 proteins for 24 hours after drug addition (table S5). Comparing protein removal with and without the drug revealed a global increase in half-lives: Most proteins (22 out of 32) increased their half-life or retained the same half-life (9 out of 32), and only one showed a decrease (Fig. 2A). Mean half-life doubled from 9.0 ± 4.6 hours to 18.8 ± 14.8 hours (paired *t* test, $P < 10^{-5}$). This effect also persisted 24 to 48 hours after drug addition (fig. S5).

Notably, the increase in half-lives showed the following pattern: Long-lived proteins became longer-lived in response to the drug, whereas short-lived proteins remained largely unaffected (Fig.

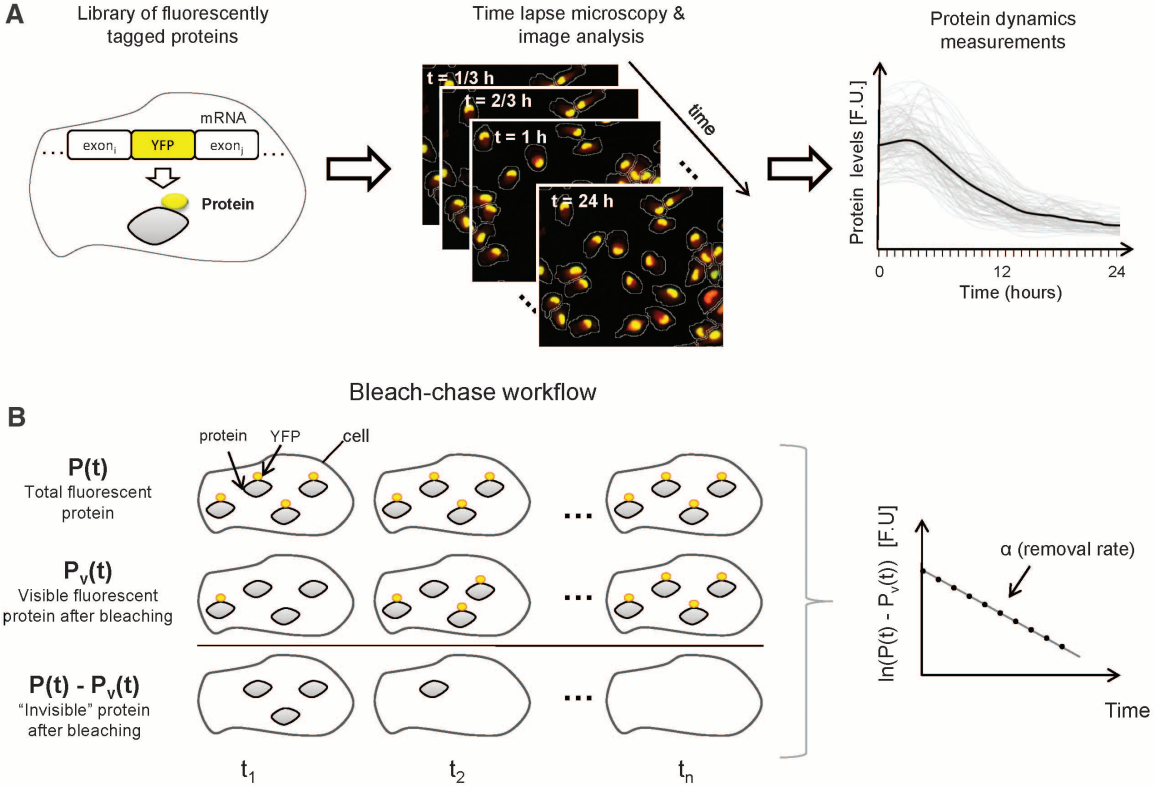

Fig. 1. Bleach-chase workflow. (**A**) Fluorescence of endogenously YFP-tagged proteins is automatically quantified from time-lapse movies (20-min resolution). Average dynamics (black) are means of ~500 individual cells (gray). (**B**) In bleach-chase, protein fluorescence dynamics is measured in bleached and unbleached cells (P_v and P, respectively). The difference between bleached and unbleached cells decays in time, with a slope on a semilogarithmic plot equal to the protein removal rate, α. Half-life is $T_{1/2} = \ln(2)/\alpha$. F.U., fluorescence units.

2A). We turn to explore possible mechanisms that can explain this effect.

The systemic increase in half-lives means that protein removal rates were globally reduced by the drug. One mechanism that could cause this decrease is down-regulation of the degradation machinery (e.g., inhibition of ubiquitin-proteasome–mediated proteolysis). However, this would not account for the differential half-life increase of long-lived proteins. On the contrary, long-lived proteins would be expected to be the least affected, because their half-lives are largely determined by dilution due to cell growth rather than by degradation (Fig. 3B and fig. S8).

An alternative explanation is that the drug stopped cell growth and thus reduced the dilution rate. Indeed, mitosis rate dropped immediately upon drug addition and halted after 5 to 7 hours. To see why growth arrest is sufficient to produce the observed half-life effect, note that growth arrest eliminates dilution, which differentially affects the protein removal rate α. Because $\alpha = \alpha_{deg} + \alpha_{dil}$, proteins with slow degradation have a larger relative reduction in α than proteins with fast degradation (described by Eqs. 4 and 5 in Fig. 2C).

This reasoning can quantitatively predict a protein's half-life after growth arrest, $T^*_{1/2}$, on the basis of its half-life before the arrest, $T_{1/2}$, and the average cell cycle duration, T_{cc} (Eq. 5 in Fig. 2C). Using the measured cell cycle duration—T_{cc} = 22.5 ± 2.6 hours and $k_2 = 0$, because the cell cycle stops after drug addition—generates predictions for the half-lives after drug addition. Note that, because the model parameters are all measured, no parameter fitting is required. The predictions (blue line in Fig. 2A) capture the measured behavior reasonably well ($P < 10^{-4}$, fig. S4). Three proteins (CD44, DDX18, and RPS3A) deviated from the general trend, with degradation rates increasing in response to the drug, which indicates specific degradation regulation (fig. S6).

To further test the generality of this effect, we measured half-life changes in response to four additional stresses: serum-starvation, the transcription inhibitor actinomycin-D, and the anticancer drugs paclitaxel and cisplatin, which reduced cell-division rates to 15, 10, 0, and 85% of the predrug rates, respectively. We found the same effect as for CPT: Long-lived proteins became longer-lived, whereas short-lived proteins remained less affected (Fig. 3, D to G, and table S6), in a way that was quantitatively predictable when we used the appropriately reduced dilution rates.

One unexpected finding is that the present cells do not appear to compensate for changes in growth rate by correspondingly altering protein degradation rates [see also (*16*)]. Consequentially, changes in growth rate directly affect protein half-lives, which results in corresponding changes in protein levels (Fig. 4A). Thus, drugs that change growth rate can cause a global imbalance in proteome levels. This imbalance is expected to be larger the faster the cells grow before the drug is administered (Fig. 4B). Proteome unbalancing may cause cell death (*17*, *18*) and, therefore, might enhance differential killing of rapidly growing cell types, such as tumors, by means of growth-arresting drugs.

Our analysis also highlights the inherent sensitivity of long-lived proteins to fluctuations in cellular growth (Fig. 4C), which suggests that one way to preserve robust levels is by maintaining proteins that are short-lived. Furthermore, to preserve stochiometry, it helps to provide pro-

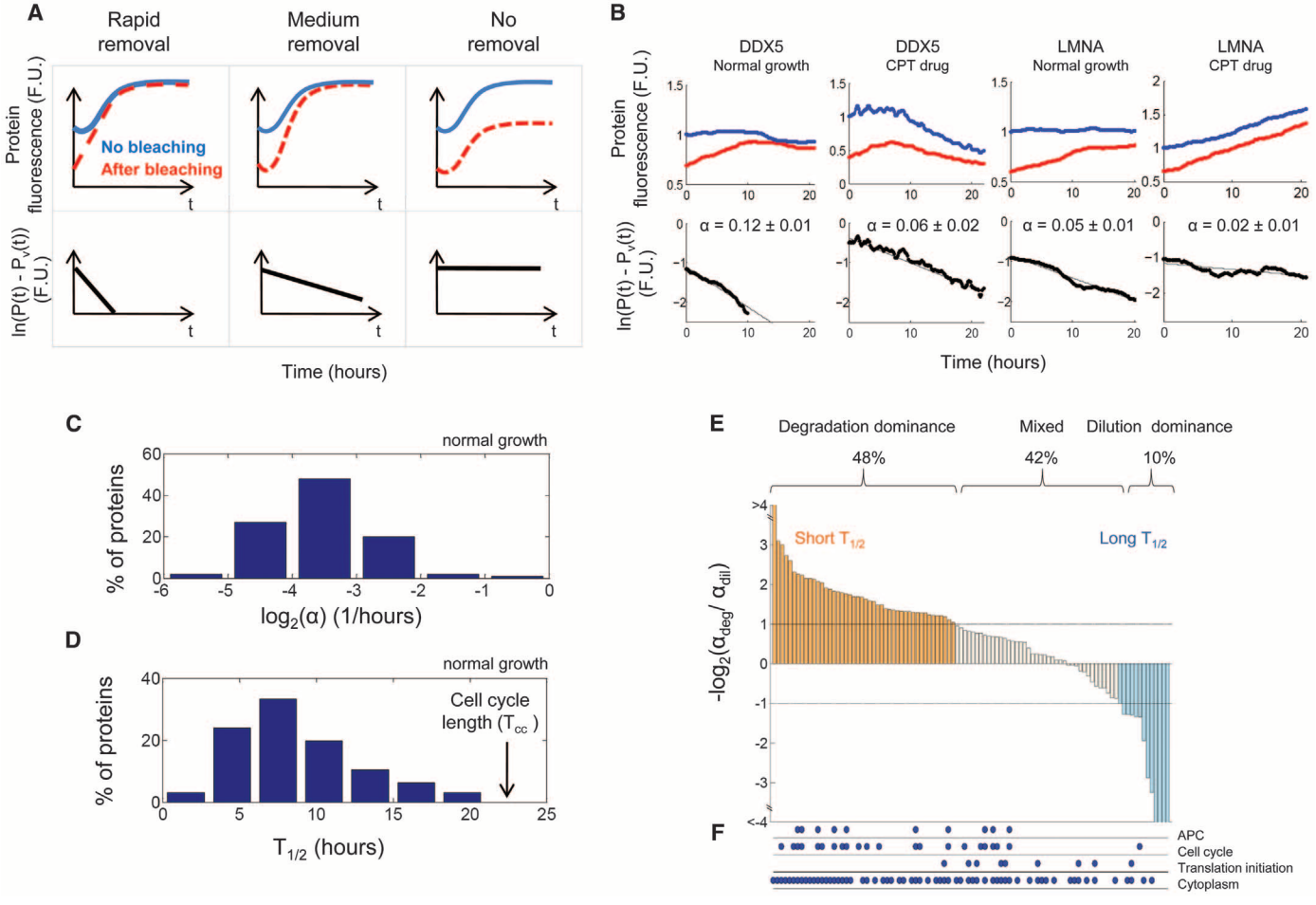

Fig. 2. The balance between degradation and dilution under normal growth varies widely between proteins. (**A**) Schematic dynamics for proteins with rapid, medium, and no removal removal rates. (**B**) Bleach-chase of two proteins in normal growth and in response to a drug. Distribution of 100 protein removal rates (**C**) and half-lives (**D**) under normal growth. α ranges between 0.03 and 0.82 with an average of 0.1 ± 0.09 (1/hour). (**E**) The balance between degradation and dilution of 100 proteins. (**F**) Proteins with similar functions or localizations tend to share similar half-lives.

teins in the same complex or system with similar degradation rates, so that fluctuations in dilution would not affect the ratio of their levels.

Elucidating the principles that govern protein removal is important for understanding how cells dynamically control their proteome. This study presents an accurate assay of protein removal and a principle by which one can understand and predict how different stresses, including chemotherapeutic drugs, affect protein removal in living human cancer cells.

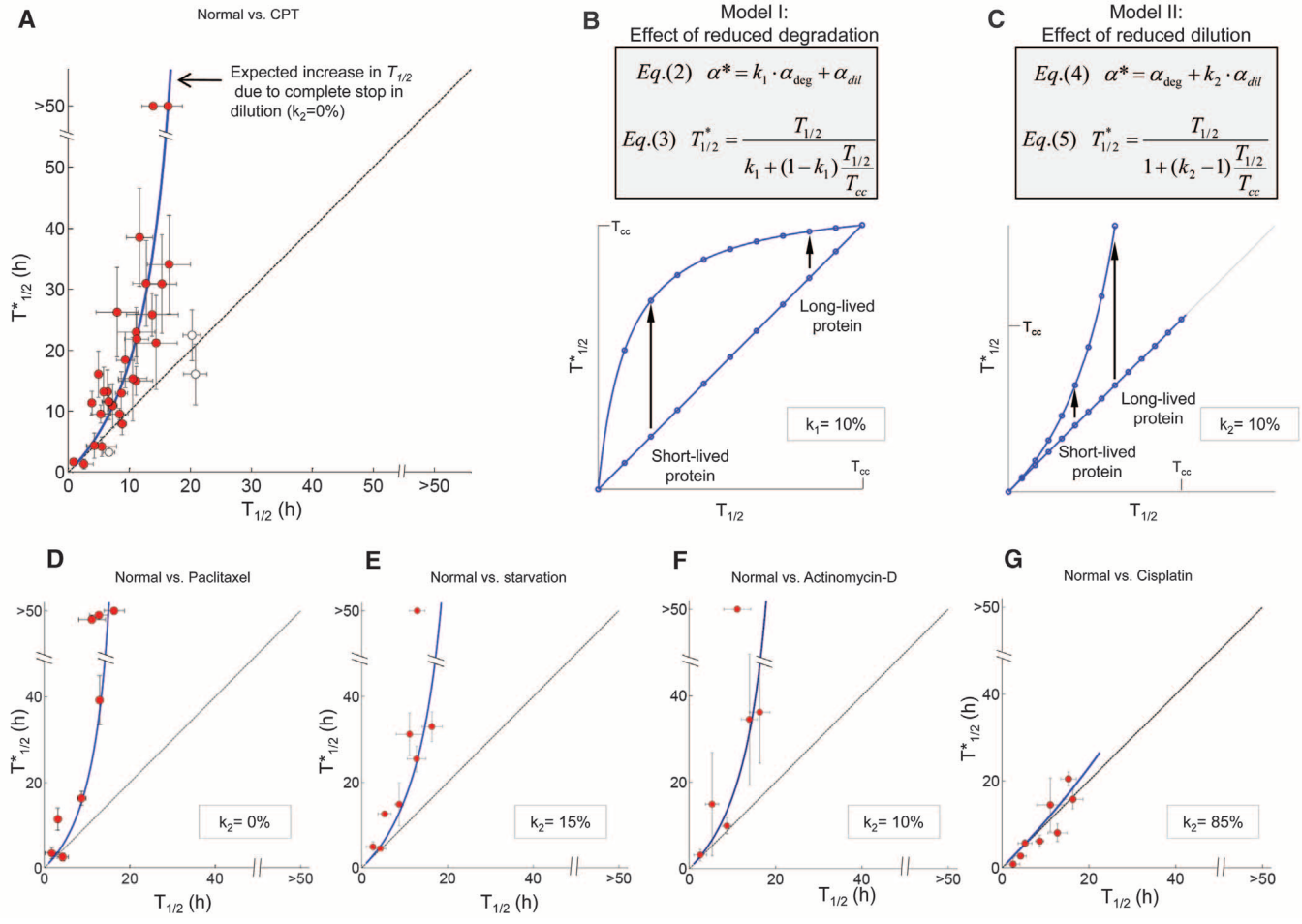

Fig. 3. Protein half-lives increase in response to stress: the longer the half-life, the larger the increase. (**A**) A comparison between half-lives under normal growth (*x* axis) and after CPT drug addition (*y* axis). Blue line is the predicted half-lives due to growth arrest (Eq. 5), with T_{cc} = 22.5 hours (measured cell cycle duration) and k_2 = 0 (growth arrest). White dots indicate proteins that significantly deviate from the line. (**B**) A model with reduced degradation (Eqs. 2 and 3) does not account for the observed half-lives, whereas a model with reduced dilution (Eqs. 4 and 5) does (**C**). (**D** to **G**) Changes in protein half-lives, comparing normal growth (*x* axis) with growth under different stresses (*y* axis), are captured by the reduced dilution model (blue lines), with k_2 equal to the measured ratio between post- and prestress growth rates.

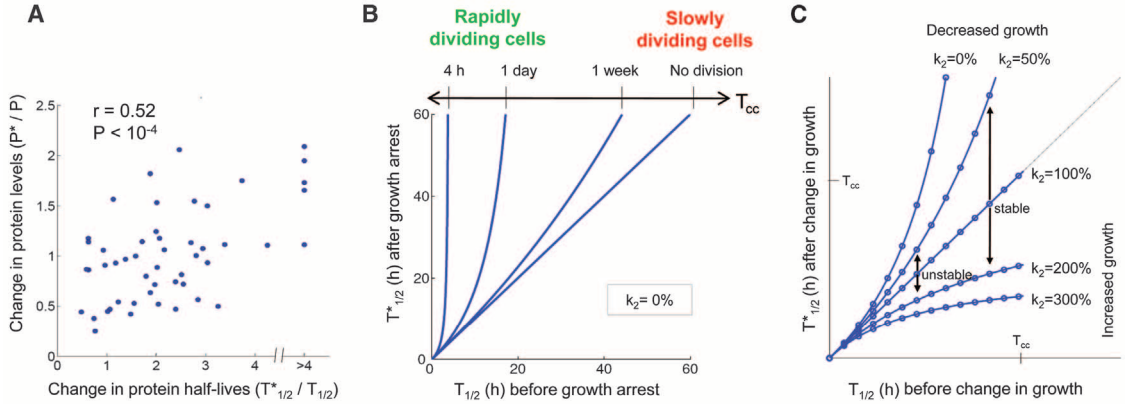

Fig. 4. The faster cells divide, the larger the expected half-life increase due to growth arrest. (**A**) Measured changes in half-lives (pre- and 24 hours post-stress) are positively correlated with changes in the corresponding protein levels. The fold increases in protein levels compared with half-lives are smaller, possibly because of decreased production rates and the fact that protein levels have not reached a steady state. (**B**) The expected half-life increase is steeper the faster cells divide before drug-caused arrest. Curves are for different T_{cc} and k_2 = 0 (Eq. 5). (**C**) The longer the protein half-life, the more sensitive it is to fluctuations in growth rate (changes in k_2, Eq. 5).

References and Notes

1. A. Ciechanover, *Nat. Rev. Mol. Cell Biol.* **6**, 79 (2005).
2. A. Hershko, A. Ciechanover, *Annu. Rev. Biochem.* **67**, 425 (1998).
3. A. L. Schwartz, A. Ciechanover, *Annu. Rev. Med.* **50**, 57 (1999).
4. K. I. Nakayama, K. Nakayama, *Nat. Rev. Cancer* **6**, 369 (2006).
5. J. M. Pratt *et al.*, *Mol. Cell. Proteomics* **1**, 579 (2002).
6. U. Alon, *An Introduction to Systems Biology* (Chapman & Hall, New York, 2007).
7. R. T. Schimke, D. Doyle, *Annu. Rev. Biochem.* **39**, 929 (1970).
8. H. C. Yen, Q. Xu, D. M. Chou, Z. Zhao, S. J. Elledge, *Science* **322**, 918 (2008).
9. J. Monod, A. M. Pappenheimer Jr., G. Cohen-Bazire, *Biochim. Biophys. Acta* **9**, 648 (1952).
10. Materials and methods are available as supporting material on *Science* Online.
11. A. A. Cohen *et al.*, *Science* **322**, 1511 (2008).
12. A. Sigal *et al.*, *Nat. Protoc.* **2**, 1515 (2007).
13. T. Surrey *et al.*, *Proc. Natl. Acad. Sci. U.S.A.* **95**, 4293 (1998).
14. O. Tour, R. M. Meijer, D. A. Zacharias, S. R. Adams, R. Y. Tsien, *Nat. Biotechnol.* **21**, 1505 (2003).
15. Y. Pommier, *Nat. Rev. Cancer* **6**, 789 (2006).
16. S. Levy *et al.*, *PLoS ONE* **2**, e250 (2007).
17. H. Liu, J. Krizek, A. Bretscher, *Genetics* **132**, 665 (1992).
18. H. Dong, L. Nilsson, C. G. Kurland, *J. Bacteriol.* **177**, 1497 (1995).

19. We thank Z. Yakhini, Z. Kam, R. Milo, S. Sela, and A. Ciechanover for discussions and P. Choukroun for technical assistance. We acknowledge support by the European Research Council, the Israel Science Foundation, and the Kahn Family Foundation. The Weizmann Institute of Science has filed for a patent on the technology described in this report for measuring protein half-lives.

Supporting Online Material

www.sciencemag.org/cgi/content/full/science.1199784/DC1
Materials and Methods
SOM Text
Figs. S1 to S9
Tables S1 to S9
References
Movie S1

29 October 2010; accepted 16 December 2010
Published online 13 January 2011;
10.1126/science.1199784

K^+ Channel Mutations in Adrenal Aldosterone-Producing Adenomas and Hereditary Hypertension

Murim Choi,[1] Ute I. Scholl,[1] Peng Yue,[2]* Peyman Björklund,[3,4]* Bixiao Zhao,[1]* Carol Nelson-Williams,[1] Weizhen Ji,[1] Yoonsang Cho,[5] Aniruddh Patel,[1] Clara J. Men,[1] Elias Lolis,[5] Max V. Wisgerhof,[6] David S. Geller,[7] Shrikant Mane,[8] Per Hellman,[4] Gunnar Westin,[4] Göran Åkerström,[4] Wenhui Wang,[2] Tobias Carling,[3] Richard P. Lifton[1]†

Endocrine tumors such as aldosterone-producing adrenal adenomas (APAs), a cause of severe hypertension, feature constitutive hormone production and unrestrained cell proliferation; the mechanisms linking these events are unknown. We identify two recurrent somatic mutations in and near the selectivity filter of the potassium (K^+) channel KCNJ5 that are present in 8 of 22 human APAs studied. Both produce increased sodium (Na^+) conductance and cell depolarization, which in adrenal glomerulosa cells produces calcium (Ca^{2+}) entry, the signal for aldosterone production and cell proliferation. Similarly, we identify an inherited *KCNJ5* mutation that produces increased Na^+ conductance in a Mendelian form of severe aldosteronism and massive bilateral adrenal hyperplasia. These findings explain pathogenesis in a subset of patients with severe hypertension and implicate loss of K^+ channel selectivity in constitutive cell proliferation and hormone production.

Aldosterone, a steroid hormone synthesized by the adrenal glomerulosa, is normally produced in two conditions, intravascular volume depletion and hyperkalemia (high plasma K^+ level) (*1*). Volume depletion activates the renin-angiotensin system, producing the hormone angiotensin II (AII), which signals via its G protein–coupled receptor (GPCR) in glomerulosa cells. The resting membrane potential is set by K^+ channel activity (*2*); both AII signaling and hyperkalemia cause membrane depolarization and activation of voltage-gated Ca^{2+} channels. Increased intracellular Ca^{2+} provides the normal signal for aldosterone production, and sustained increases lead to glomerulosa cell proliferation (*1*, *3*–*5*); AII also causes increased inositol 1,4,5-trisphosphate (IP_3) and transient Ca^{2+} release from intracellular stores. Aldosterone signaling in the kidney increases electrogenic Na^+ reabsorption, defending intravascular volume, and also increases K^+ secretion.

In primary aldosteronism, the adrenal gland constitutively produces aldosterone in the absence of AII or hyperkalemia, resulting in hypertension and variable hypokalemia (low plasma K^+ level). Primary aldosteronism is found in ~10% of patients referred for evaluation of hypertension. A third or more of these have aldosterone-producing adenoma (APA, also known as Conn's syndrome) of the adrenal cortex (*6*); of the remainder, a small fraction have mutations that cause constitutive expression of aldosterone synthase (*7*), and the rest are classified as idiopathic.

APAs are typically solitary, well circumscribed, and diagnosed between ages 30 and 70 (*8*). They come to medical attention due to new or worsening hypertension, often with hypokalemia. Aldosterone is elevated while renin levels are suppressed (reflected in a high aldosterone:renin ratio), and a characteristic adrenal mass is seen on computed tomography (CT). Adrenal vein sampling demonstrates predominant aldosterone secretion from the gland harboring the tumor. APAs virtually always remain benign, without local invasion or distant metastasis (*9*). Surgical removal ameliorates or cures hypertension in the large majority of patients (*10*). The mechanisms responsible for neoplasia and cell-autonomous aldosterone production are unknown.

We studied 22 patients with APA (table S1) (*11*). All came to medical attention with hypertension and variable hypokalemia. All had high aldosterone:renin ratios and unilateral adrenal cortical mass on CT. At surgery, adrenocortical tumors of mean diameter 2.8 cm were removed, and pathology in all cases confirmed adrenocortical adenoma.

Genotyping of tumors on Illumina 1M-Duo chips demonstrated two gross classes of tumors: those with zero or few chromosome arms with loss of heterozygosity (LOH) (11 with none, 3 with 1 to 4 LOH events) and those with many large LOH segments (8 with 11 to 19 LOH segments) (table S1 and fig. S1). Subjects with low LOH tumors tended to be younger with smaller tumors.

We performed whole exome capture and Illumina sequencing on four APA-blood pairs from unrelated subjects with no LOH segments. Each tumor sample was assessed by histology to be free of normal adrenal cells; some admixture with blood and stromal cells is inevitable, and we accordingly sequenced samples to high depth of coverage to enable detection of somatic mutations. The mean coverage of each targeted base was 183-fold for blood DNA and 158-fold for tumor DNA, and 97% of all targeted bases in tumor samples were read at least eight times (table S2). We identified high-probability somatic mutations in each tumor ($P = 10^{-4}$ to 10^{-56} of chance occurrence) (fig. S2), and confirmed each by direct Sanger sequencing

[1]Departments of Genetics and Internal Medicine, Howard Hughes Medical Institute, Yale University School of Medicine, New Haven, CT 06510, USA. [2]Department of Pharmacology, New York Medical College, Valhalla, NY 10595, USA. [3]Department of Surgery, Yale Endocrine Neoplasia Laboratory and Yale Cancer Center, Yale University School of Medicine, New Haven, CT 06510, USA. [4]Department of Surgical Sciences, Uppsala University, Uppsala, Sweden. [5]Department of Pharmacology, Yale University School of Medicine, New Haven, CT 06510, USA. [6]Division of Endocrinology, Henry Ford Hospital, Detroit, MI 48202, USA. [7]Section of Nephrology, Yale University School of Medicine, and Department of Medicine, Veterans Affairs Medical Center, West Haven, CT 06516, USA. [8]Yale Center for Genome Analysis, Yale University School of Medicine, West Haven, CT 06516, USA.

*These authors contributed equally to this work.
†To whom correspondence should be addressed: E-mail: richard.lifton@yale.edu